

NON-DESTRUCTIVE CHARACTERIZATION OF DEER (*CERVUS ELAPHUS*)
ANTLERS BY X-RAY MICROTOMOGRAPHY COUPLED WITH IMAGE ANALYSIS

A. Léonard^{1*}, L. Guiot², J.-P Pirard¹, M. Crine¹, M. Balligand², S. Blacher¹

¹Laboratory of Chemical Engineering, Department of Applied Chemistry,
University of Liège, B6 – Sart Tilman, 4000 Liège, Belgium

²Department of Clinical Sciences, Faculty of Veterinary Medicine,
University of Liège, B44 – Sart Tilman, 4000 Liège, Belgium

*Correspondence: A. Léonard. Tel. +32 4 366 47 22; Fax: +32 4 366 28 18; e-mail:
a.leonard@ulg.ac.be.

ABSTRACT

X-ray microtomography coupled with image analysis was tested as a non-destructive alternative method for the textural characterization of the trabecular part of deer antlers (*Cervus Elaphus*). As gas adsorption and mercury intrusion can not be applied on this soft and spongy material, its pore texture was, up to now, determined from histological sections which give only two dimensional information. In this work, x-ray microtomography is used to scan entire or half pieces of antlers and 3D image analysis is performed in order to assess the differences between samples collected at various antler locations. Results clearly show

a porosity profile along the sample diameter. The pore size distribution is showed to be dependent on the sample original site.

INTRODUCTION

The antlers of cervids are constituted of bone tissue covered with velvet in the early stage of growth. In the literature, the bone tissue is described as a central core of spongy bone surrounded by a thick outer layer of compact bone, as summarized in the review of Crigel et al. (2001). Rolf and Enderle (1999) defined four different histological zones in a transversal cross section. From the periphery to the center, there are: the subvelvet zone made of osteoids, the zone of osteonic bone made of compact lamellar bone, the transition zone from osteonic to trabecular bone, and finally the central spongiosa zone constituted of trabecular bone. The two outer regions are very dense and compact, while the center presents a general honeycombed structure.

Since deer antlers can withstand large stresses, they represent a great interest to both biomedical and material scientists. It is well-known that the mechanical properties of porous material greatly depend on the pore size and their connectivity (Gibson & Ashby, 1997). Recently, Evans et al. (2005) studied in details the pore structure of fallow deer (*Dama Lama*) antlers in the range from ~1 nm to ~100 μm using NMR spectroscopy, gas adsorption and mercury intrusion techniques. According to the pore size range investigated, this study mainly concerned osteonic bone and no the trabecular part. However, the deep knowledge of the pore arrangement of the spongy bone (pore width larger than 100 μm) is

also of high importance. Indeed, the mechanical and structural properties of both the spongiosa and transition regions make antler central part a good candidate to be used as biomaterial in orthopaedics (Crigel et al., 2001). The particular porous structure of the spongy zone, which depends on several factors such as species, age, feeding, location along the antler, has to be precisely probed.

Up to now, the pore structure of the trabecular part was assessed from the analysis of TEM histological sections or merely by SEM surface observations. In addition to sampling limitations, these methodologies fail to describe the whole 3D morphology. Mercury porosimetry is commonly used to measure pore volume and pore size distribution of high porous materials. However, in some cases (Maquet et al., 2003) this method presents the following limitations: (i) mercury porosimetry is limited to maximum pore sizes of 75 μm , (ii) if the porous structure is widely open, the mercury does not intrude the sample but flows through the porous structure, hindering any measurement, (iii) soft materials collapse under mercury pressure instead of being intruded. For antlers, optical microscopy observations showed pore widths larger than 200 μm in the spongy zone, *i.e.* out of range (Evans et al., 2005). Moreover the structure is complex and widely open to enable internal vascularisation. Finally, the spongy material is very soft, *i.e.* any cutting operation will affect its pore structure and it will probably collapse during mercury porosimetry measurements. As this latter technique can not be applied, x-ray microtomography coupled with image analysis is proposed in this work as a non-destructive alternative method for the 3D characterization of the spongy center of deer antlers. The results are compared with image analysis measurements performed on 2D histological sections. This study focuses on

red deer (*Cervus Elaphus*) which is a widespread species in northwestern Europe, namely in Ardenne (Belgium). From a methodological point of view, this work concerning antler trabecular part can be considered as complementary to that of Evans et al (2005) that studied in depth the pore structure of antler cortical part for another species.

MATERIALS AND METHODS

Sample preparation

The deer (*Cervus Elaphus*) antler samples were collected before antler casting, during the active growth phase when they are still covered by velvet. The samples, made principally of primary bone tissue, were machine-turned from the core of the antler main beam, at two different levels (samples A and B). Once shaped, the cylinders were washed with tap water under high pressure and eventually cleaned with hydrogen peroxide.

Optical Microscopy

After hydrogen peroxide cleaning and drying, sections of 1 cm were fixed in a 4 % paraformaldehyde solution (Polysciences, Inc., Warrington, PA) during 3 to 4 h at room temperature. Then samples were washed with tap water, decalcified (one night in Decalcifiant medium, DC2, Labonord) and embedded in paraffin. Histological sections of 4 μm thick were cut and stained with hematoxiline-eosine. Micrographs were taken with a microscope Leica (Van Hopplynus, Germany).

X-ray microtomography

X-ray microtomography is a non-invasive technique allowing the visualization of the internal texture of a material. The x-ray tomographic device used in this study is a “Skyscan-1074 X-ray scanner” (Skyscan, Belgium). Advanced technical details about its conception and operation are described by Sasov and Van Dyck (1998). The X-ray source operated at 40 kV and 1 mA. The detector was a 2D, 768 pixels \times 576 pixels, 8-bit X-ray camera with a pixel size of 41 μ m. The rotation step was fixed at the minimum, 0.9°, in order to improve image quality. In contrary to classical medical scanner, the source and the detector were fixed, while the sample was rotated during the measurement. Once the sample was placed into the microtomograph, the scanning was performed, allowing the investigation of a height of max 25 mm. Cross sections separated by 205 μ m were reconstructed using a cone-beam reconstruction software.

IMAGE ANALYSIS

Image processing and measurements

3D tomographic images

The 3D images of samples were built by stacking *ca.* 100 cross sections obtained by X-ray microtomography. They must be processed as a single object. The resulting 3D grey levels

image is formed by two phases: the pore space at low grey levels (dark voxels), and the bone skeleton at high grey levels (bright voxels).

Image analysis quantification was first performed on the original grey-level 3D images. As the real structure of the antlers could be blurred by noise in the un-processed tomograms, the tomograms were also binarized. The same analysis was carried out on both binary and grey-level images and the results were compared.

The aim of binarization is to determine to which phase each voxel of the 3D image belongs. This is particularly difficult in the transition zone between phases in which the difference between grey tones is not sharp. Then, to increase the contrast a combination of top-hats contrast operators (Serra, 1982) were first applied. The morphological white/black top-hat (WTH/BTH) is defined as the difference between the original image and its opening/closing by a given structuring element. The addition of the original image (I) to its WTH transformed image, $I_1 = I + WTH(I)$, enables to enhance bright objects (bone skeleton) and the subtraction from the resulting image I_1 of the BTH transformed original image, $I_{TH} = I_1 - BTH(I)$, enables to enhance the dark objects (pore space) (Soille, 1999). For all this morphological transformations, spherical structuring element was approached by an octahedron of size 1 corresponding to a $3 \times 3 \times 3$ neighborhood.

The contrast enhanced image was further thresholded by assigning the value 1 to all pixels whose intensity is below a given grey tone value and 0 to the others. The optimum threshold was determined as follows: a threshold was calculated for each slice using the method of Otsu (1979). With this method, the threshold level is chosen automatically so as to maximize the interclass variance and to minimize the intraclass variance of the thresholded black (pores) and white (bone) pixels. The obtained slice threshold values were

very close which indicates that the grey level structure is rather homogeneous. Figure 1a and 1b show typical grey level cross section and its corresponding binary one. Finally, the mean of the slice threshold values was calculated and the same value was used for all slices.

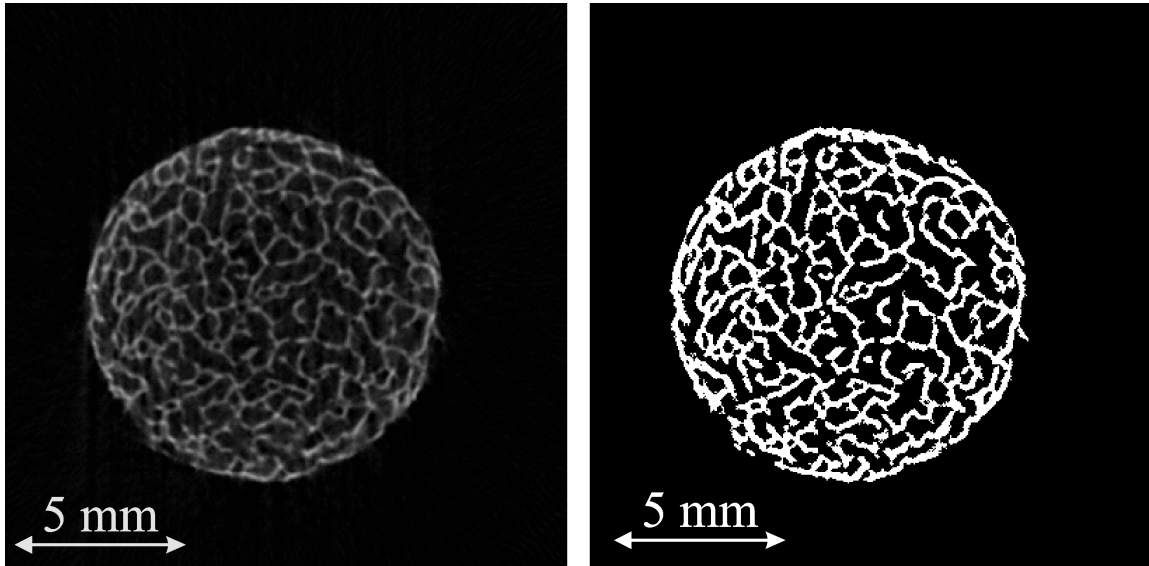


Figure 1. (a) Typical grey level cross section of sample A, (b) corresponding binary image.

Quantification of the 3D grey-level and binary images follows the same line as previous works related to the characterization of highly porous materials (Blacher et al., 2004; Léonard et al., 2005). The following measurements were performed:

On the grey-level images:

a) The grey-level density distribution. This is defined as the sum of the grey-level intensity of all pixels within a layer located at a distance d from the center of the sample, divided by the value of the same sum if all pixels in the layer had the maximum intensity. For this measurement, the shape of the layers is critical; it must be chosen as a function of the pore structure and of the shape of the sample. As the 3D visualization of the samples revealed a roughly isotropic structure, layers were defined by the volume in between successive

cylinders (see inset in Figure 4a).

b) The grey-level opening granulometry: Opening is an operation of mathematical morphology that uses a geometrical object called structuring element with which the image is compared. Let the intensity function $I(x,y,z)$ be a 3D image and B a 3D structuring element of size λ (a sphere, a cube, etc.). In a 2D space, the image $I(x,y)$ can be visualized as a topographic map in which the grey level I corresponds to an altitude. The principle of grey-level opening granulometry is described and illustrated in reference (Gommes et al., 2006). Briefly, applying an opening transformation to an image $I(x,y,z)$ with B of size λ produces a modified image $I'(x,y,z) < I(x,y,z)$ in which all the maxima of I that cannot be included in B have been removed. The average value I_{avg} of $I(x,y,z)$ after successive opening transformations is a decreasing function of λ . The position of maxima in the derivative $-dI_{avg}/d\lambda$ corresponds to the characteristic length of the image.

On the binary images:

a) The total porosity (ϵ'), defined as $\epsilon' = \text{number of pixels characteristic of the pores } (V_p) / (\text{number of pixels characteristic of the pores} + \text{number of pixels characteristic of the bone})$.

To determine the total volume of the sample the bounding box of the bone skeleton was built.

b) The pore density distribution measured on binary images defined as the number of pixels characteristic of the pores in a layer located at a distance d from the center of the sample divided by the total number of pixels that form that layer. The same concentric layered masks were used as for the determination of the grey-level intensity distribution (inset in Figure 4a).

(c) Binary opening granulometry. As the pores have a continuous structure, made of a

single object, standard granulometry cannot be applied. Therefore opening size granulometry (Serra, 1982) was performed, as done previously on the grey-level images. When an opening transformation is carry out on a black and white (binary) image with a structuring element of size λ , objects (or parts of objects) with a size smaller than λ are removed. After successive opening transformations with increasing sizes λ , the volume of the image V , *i.e.* the total number of white voxels, decreases. The position of maxima in the derivative $-dV/d\lambda$ corresponds to the characteristic length of the image.

2D Optical microscopy images

2D grey level images obtained by optical microscopy were first binarized using the Otsu's method (1979). Figure 2 shows the images corresponding to the two samples A and B and their corresponding binary images. Quantification on 2D binary images, Figures 1(b,d), consists in measuring the total porosity (ϵ) defined as $\epsilon = \text{number of pixels characteristic of the pores } (S_p) / (\text{number of pixels of the whole image})$.

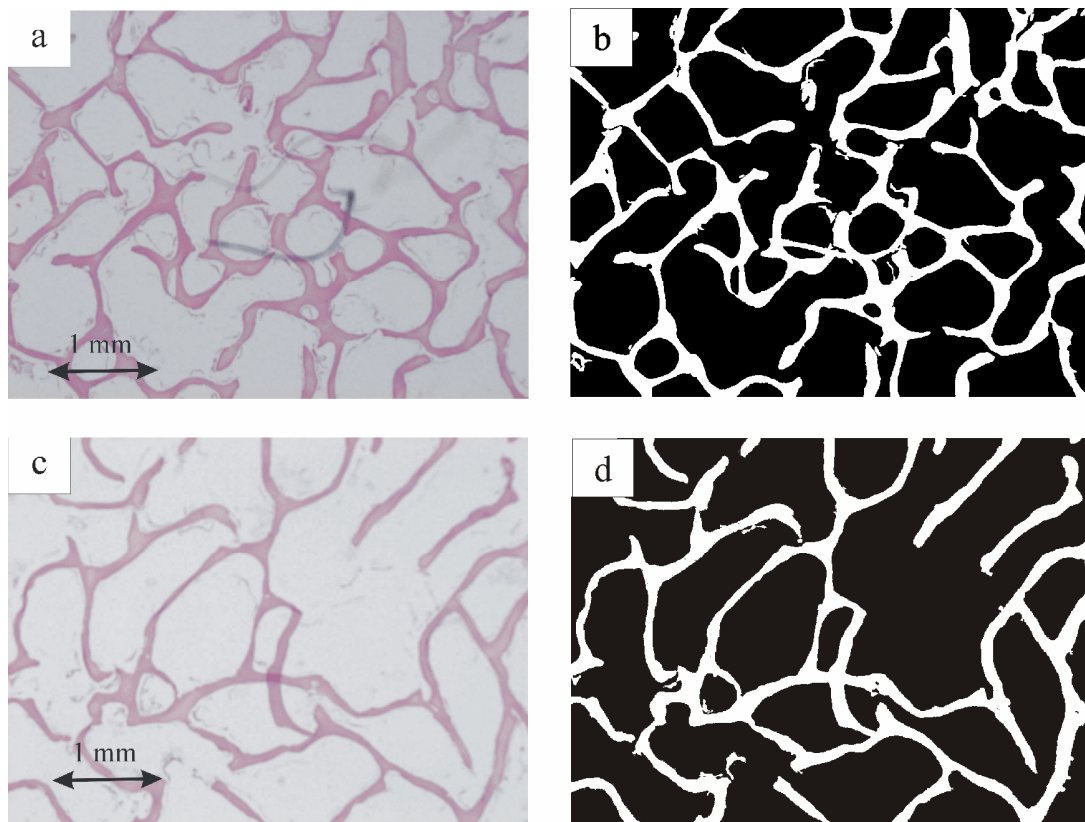


Figure 2. 2D images obtained by optical microscopy of sample A (a) and B (c) and the corresponding binary images (b), (d).

RESULTS

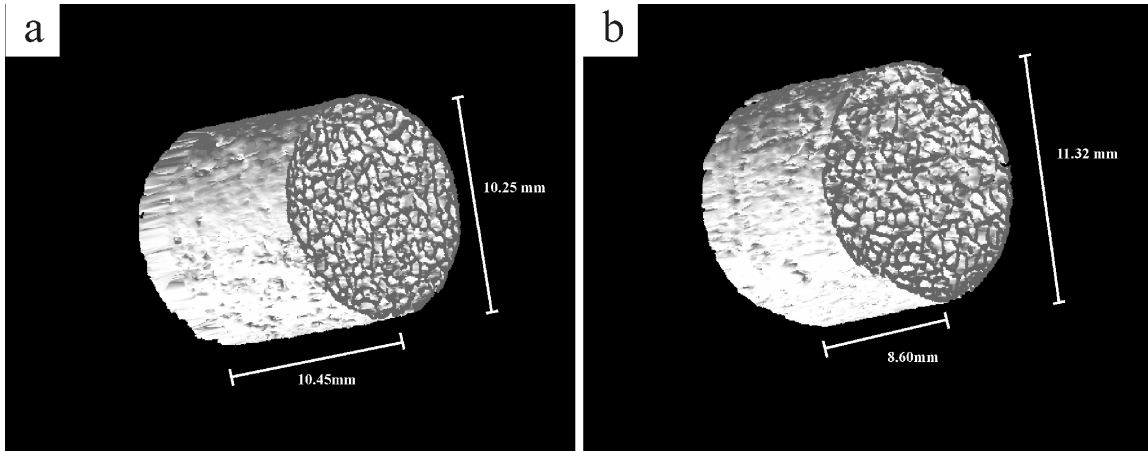


Figure 3. 3D images obtained by microtomography of pieces of deer antlers, (a) sample A, (b) sample B.

The 2D measurements of porosity obtained from 2D binary images (see examples in Figures 2(b,d)) give $\epsilon_A=0.74$ and $\epsilon_B=0.79$. The 3D measurements of porosity, obtained from 3D binary image, Figures 3(a,b), $\epsilon'_A = 0.63$ and $\epsilon'_B = 0.66$, are lower than the 2D counterparts but it follows the same trend. To explain this discrepancy, the internal structure of the deer (*Cervus Elaphus*) antlers must be investigated. For the two samples, the pore density function increases from the boundary to the center, Figures 4 (a,b), which indicates that the pore structure is not homogeneous. The 2D measurement of porosity is close to the porosity near the center of the deer antlers whereas the 3D porosity measurement gives a mean value over the whole sample. Then, the disagreement between the 2D and 3D porosity can be attributed to the appropriate choice of sampling, usually encountered with 2D measurements.

Figures 4a and b compare the grey-level intensity distribution to the pore density distributions, for the two samples respectively. For each sample, the two kinds of profiles (grey-level and binary) exhibit almost the same periodicity, with maxima and minima being almost superimposed. However, the variations of binary profiles are more marked as they describe the abrupt transitions between skeleton and pores.

Although the total porosities of the samples are very close, their pore structures are quite different. Indeed, the pore density function of sample A exhibits a clear periodicity (Figure 4a) in which the distance between maxima represents the distance between bonds, whereas for sample B the curve is smoother. To quantify these periodicities, the power spectra of the pore density distributions, that exhibit more pronounced variations than the grey level ones, were determined. For the two samples, the peak close to the origin probably results from the leakage of the constant component of the function. For samples A and B, Figures 4(c,d) main peaks at $\omega_A=14.91$ (1/mm) and $\omega_B=9.67$ (1/mm) surrounded by their harmonics, are observed. These frequencies correspond to characteristic lengths ($\lambda= 2\pi/f$) of $\lambda_A= 0.42$ mm and $\lambda_B= 0.65$ mm, respectively. This means that the pores are more spaced in sample B than in sample A.

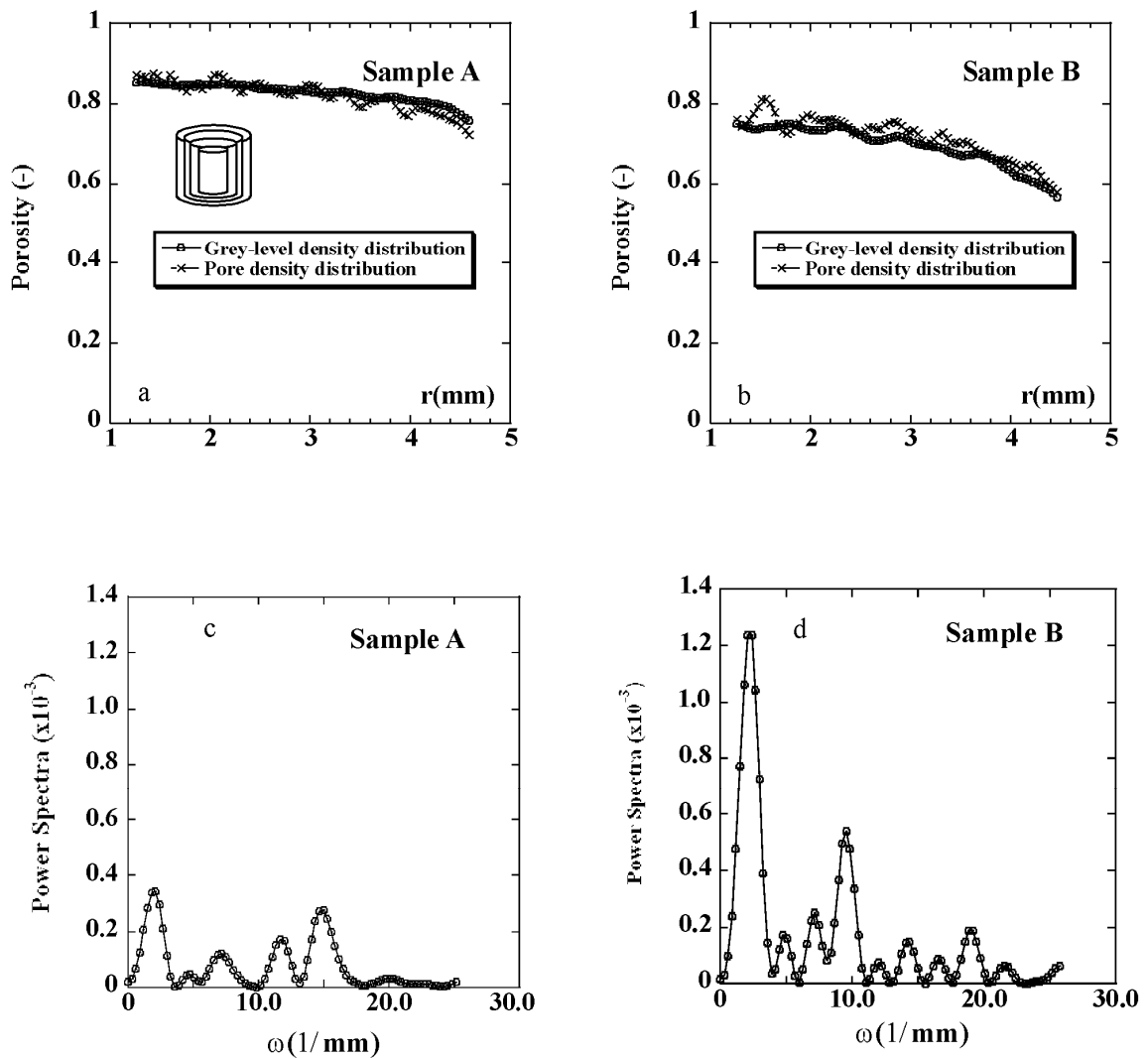


Figure 4. Pore and grey-level density distribution of (a) sample A and (b) sample B. The inset shows layers in between successive cylinders, in which the successive pore density was calculated. Power spectra of pore density distributions of samples (c) A and (b) B.

These results are confirmed by the measurement of the pore size distribution obtained by both grey-level and binary opening granulometry (Figures 5a and b). Indeed, from both the both grey-level and binary processing, the granulometry curves of sample B are shifted towards higher sizes compared to those of sample A. As expected, this trend is even more

striking for the binary treatment. Distributions are characterized by the mean, the median, the standard deviation, and the interquartile range (Iqr). Those parameters are usually used to describe empirical distributions.

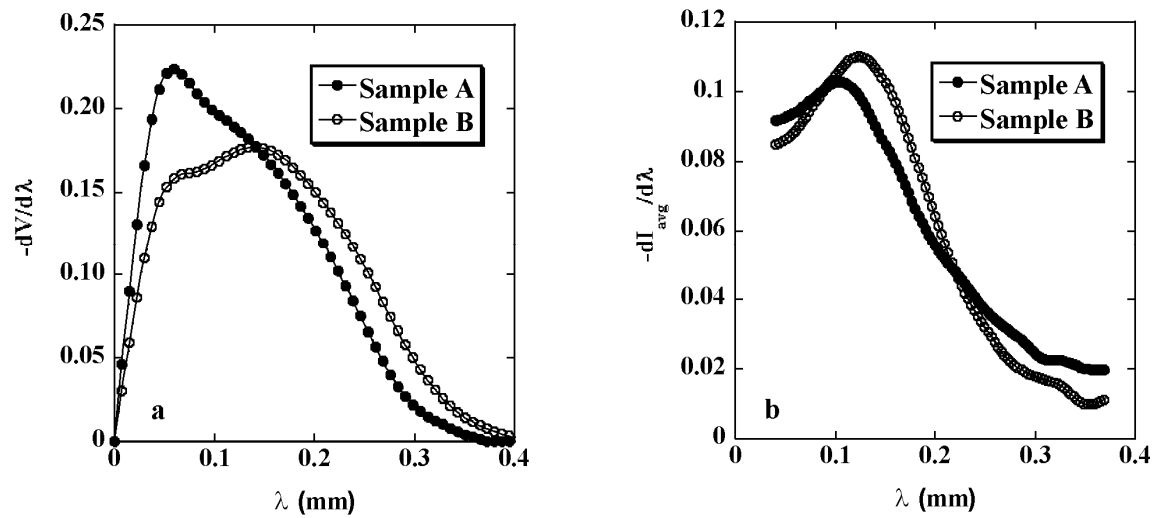


Figure 5. Binary (a) and grey-level (b) opening granulometry for samples A and B.

Statistical parameters presented in Table 1 indicate that the pore distribution of sample B is wider than the counterparts of sample A and that it spreads toward larger pore sizes. Concerning the lower values of the mean and median obtained from the binary opening granulometry in relation with the characteristic length obtained from the pore density function, it must be noticed that, by construction, the opening granulometry method induce a shift of the true size distribution towards lower values. For example, if a pore is formed by two parts nearly convex separated by a thin “isthmus”, it will be transformed after an opening transformation into two pores of lower diameter. In this case, an artificial decrease of the average diameter distribution is produced. A high decrease corresponds to a high degree of pores irregularity. In fact, this kind of measurement is especially useful for

comparative studies. Nevertheless, results confirm a recent study (to be published) based on histological sections. The total porosity and the pore size depend on the sample localization along the antler. This is a crucial information in order to select sampling site for specific biomaterials applications.

Table 1. Quantification of deer (*Cervus Elaphus*) antlers

| Measurements | Samples | |
|----------------------|------------------------------|------------------------------|
| | A | B |
| ε | 0.74 | 0.79 |
| ε' | 0.63 | 0.66 |
| λ | 0.42 | 0.65 |
| Mean \pm Std* (mm) | 0.15 \pm 0.07 ^a | 0.16 \pm 0.08 ^a |
| | 0.13 \pm 0.07 ^b | 0.15 \pm 0.08 ^b |
| Median* (mm) | 0.10 ^a | 0.12 ^a |
| | 0.18 ^b | 0.21 ^b |
| Iqr* (mm) | 0.15 ^a | 0.19 ^a |
| | 0.16 ^b | 0.18 ^b |

ε = 2D porosity; ε' = 3D porosity; λ =characteristic length between bonds; * Statistical parameters of grey-level^a and binary^b open size distribution

CONCLUSIONS

The 3D pore structure of the trabecular part of deer (*Cervus Elaphus*) antlers was successfully characterized by X-ray microtomography coupled with image analysis. This non destructive technique presents several advantages in comparison with traditional 2D imaging. The microtomograph allows probing large pieces of antler, giving good resolved images. 3D image analysis characterization enables to perform global measurements like the total porosity as well as measurements like pore density distribution and opening size granulometry, which give local information. With measurements performed at scales larger than 100 μm , x-ray microtomography constitutes an efficient complement to traditional techniques, showing the way towards multiscale analysis of porous materials.

3D image analysis was performed on both original grey-level and on binary processed images. The two methods have their pros and cons. The use of original grey-level images enables to avoid introducing modifications in the image resulting from image processing. On the other hand, as morphological features are embodied in the gradations of grey-levels, the measurements are quite dependent on the quality the original images, *i.e.* contrast, luminosity, noisiness, etc. Binary image processing leads to well delimited structures whose sizes can be accurately determined. However, in addition to being time-consuming, binarization could lead to a modification or even a loss of the information contained in the original image. In the present study the quantification of both the original grey-level and of binarized images show the same trends.

In the pore size range investigated, morphological differences between antler samples cut at different levels were clearly established. Further work is currently carried out in order to study the influence of several parameters (sampling site, deer's age, ...) on the textural properties of deer (*Cervus Elaphus*) antlers. This is an essential step to realize an optimal sample selection (in term of porosity, mechanical properties, ...) for biomaterial applications.

ACKNOWLEDGEMENTS

A. Léonard is indebted to the Belgian Fonds National de la Recherche Scientifique (FNRS) for a position of Postdoctoral Researcher. S. Blacher acknowledges the ALFA Program of the E.U. (project ALFA II 0412 FA FI) for enabling fruitful exchanges. The authors thank R.-M. Paquay and Professor M.-P. Defresne (Laboratory of Histology and Cytology of the University of Liège) for the realization of the optical microscopy images and their kind collaboration, and Dr. C.J. Gommaes (Department of Chemical Engineering, University of Liège) for interesting discussion.

REFERENCES

Blacher, S., Léonard, A., Heinrichs, B., Tcherkassova, N., Ferauche, F., Crine, M., Marchot, P., Loukine, E. & Pirard, J.P. (2004) Image analysis of X-ray microtomograms of Pd-Ag/SiO₂ xerogel catalysts supported on Al₂O₃ foams. *Colloid Surface A*, **241**, 201-206.

- Crigel, M.H., Balligand, M. & Heinen, E. (2001) Deer antler: scientific review. *Ann. Med. Vet.*, **145**, 25-38.
- Evans, L.A., McCutcheon, A.L., Dennis, G.R., Mulley, R.C. & Wilson, M.A. (2005) Pore size analysis of fallow deer (*Dama dama*) antler bone. *J. Mater. Sci.*, **40**, 5733-5739.
- Gibson, L.J. & Ashby, M.F. (1997) *Cellular solids. Structure and properties - Second Edition*. Cambridge University Press, Cambridge, UK.
- Gommes C. J., Basiura M., Bart Goderis B., Pirard J.-P., Blacher S. (2006) Structure of silica xerogels synthesized with organoalkoxysilane co-reactants hints at multiple phase separation. *J. Phys. Chem.*, **110**, 7757-7765.
- Léonard, A., Blacher, S., Marchot, P., Pirard, J.P. & Crine, M. (2005) Image analysis of X-ray microtomograms of soft materials during convective drying: 3D measurements. *J. Microsc.*, **218**, 247-252.
- Maquet, V., Blacher, S., Pirard, R., Pirard, J.P., Vyakarnam, M.N. & Jerome, R. (2003) Preparation of macroporous biodegradable poly(L-lactide-co-epsilon-caprolactone) foams and characterization by mercury intrusion porosimetry, image analysis, and impedance spectroscopy. *J. Biomed. Mater. Res. Part A*, **66**, 199-213.
- Otsu, N. (1979) A Threshold Selection Method from Gray-Level Histograms. *IEEE Trans. Syst. Man Cybern.*, **9**, 62-66.
- Rolf, H.J. & Enderle, A. (1999) Hard fallow deer antler: A living bone till antler casting? *Anat.l Rec.*, **255**, 69-77.
- Sasov, A. & Van Dyck, D. (1998) Desktop X-ray microscopy and microtomography. *J. Microsc.*, **191**, 151-158.

Serra, J. (1982) *Image analysis and mathematical morphology*, Vol.Vol 1. Academic Press, New York.

Soille, P. (1999) *Morphological Image Analysis – Principles and Applications*. Springer-Verlag, New York.